Strong Coupling and Degeneracy Effects in Inertial Confinement Fusion Implosions

S. X. Hu,[1,*] B. Militzer,[2] V. N. Goncharov,[1] and S. Skupsky[1]

[1]*Laboratory for Laser Energetics, University of Rochester, 250 East River Road, Rochester, New York 14623, USA*

[2]*Departments of Earth and Planetary Science and of Astronomy, University of California, Berkeley, California 94720, USA*

(Received 4 December 2009; published 10 June 2010)

Accurate knowledge about the equation of state (EOS) of deuterium is critical to inertial confinement fusion (ICF). Low-adiabat ICF implosions routinely access strongly coupled and degenerate plasma conditions. Using the path integral Monte Carlo method, we have derived a first-principles EOS (FPEOS) table of deuterium. It is the first *ab initio* EOS table which completely covers typical ICF implosion trajectory in the density and temperature ranges of $\rho = 0.002$–1596 g/cm^3 and $T = 1.35$ eV–5.5 keV. Discrepancies in internal energy and pressure have been found in strongly coupled and degenerate regimes with respect to *SESAME* EOS. Hydrodynamics simulations of cryogenic ICF implosions using the FPEOS table have indicated significant differences in peak density, areal density (ρR), and neutron yield relative to *SESAME* simulations.

DOI: 10.1103/PhysRevLett.104.235003 PACS numbers: 52.25.Kn, 52.57.−z, 52.65.Pp, 62.50.−p

As one of the potentially viable ways to generate clean energy, inertial confinement fusion (ICF) has been pursued for decades [1]. In "hot-spot" ICF designs, a cryogenic deuterium-tritium (DT) capsule is driven to implode either directly by intense laser pulses [2] or indirectly by x rays in a hohlraum [3]. At the stagnation stage, a high-density shell ($> 1000\times$ solid DT density) is assembled around the hot spot for the fusion burn to propagate, thereby generating a net energy gain. To reach such high compression, the imploding shell must stay on a low adiabat (α, the ratio of the fuel pressure to the Fermi-degeneracy pressure). Accurate knowledge of the equation of state (EOS) of the DT fuel is essential for ICF designs [1] because the compressibility is determined by the EOS [4].

Dynamically compressed by shocks and/or adiabatic compression waves driven by laser ablation [5], the imploding DT shell undergoes a wide range of plasma conditions at densities from $\sim$1.0 up to 1000 g/cm^3 and at temperatures varying from a few to several hundreds of electron volts [1]. One may expect such plasmas to enter the strongly coupled and degenerate regimes, where many-body effects become important. Such conditions are indeed accessed in low-adiabat cryogenic implosions on the OMEGA Laser System [6], as well as at the National Ignition Facility (NIF) [7]. Examples from hydrosimulations are shown in Figs. 1(a)–1(c) for a low-adiabat ($\alpha \approx 2.5$) cryo-DT implosion on OMEGA, and in Figs. 1(d), 1(c), and 1(f) for a direct-drive ignition design for the NIF. In panels (a) and (d), we plotted the laser pulse shapes. Our hydrocode simulations show that the predicted density (ρ) and temperature (T) "paths" of the driven DT shell, which are plotted in the middle panels [(b) and (e)], undergo a variety of drive stages, including several shocks and the final push by the main pulse. If we cast the ρ-T history of the imploding DT shell onto a plane spanned by the coupling parameter $\Gamma = 1/akT$ (where a is the Wigner-Seitz radius and k is the Boltzman constant) and the degeneracy parameter $\theta = T/T_F$ (where T_F is the Fermi temperature), we find that the imploding shell indeed enters the strongly coupled ($\Gamma > 1$) and degenerate ($\theta < 1$) regimes.

The effects of strong coupling and degeneracy in ICF plasmas have recently attracted much attention since they may redefine the so-called "1D physics" of ICF implosions. For example, the essential pieces of physics models used in ICF hydrosimulations, such as the electron-ion energy relaxation rate [8], the thermal conductivity [9], and the fusion rate [10] in coupled and degenerate plasmas, have been reexamined recently. In recent experiments, the EOS of liquid deuterium along the principal Hugoniot

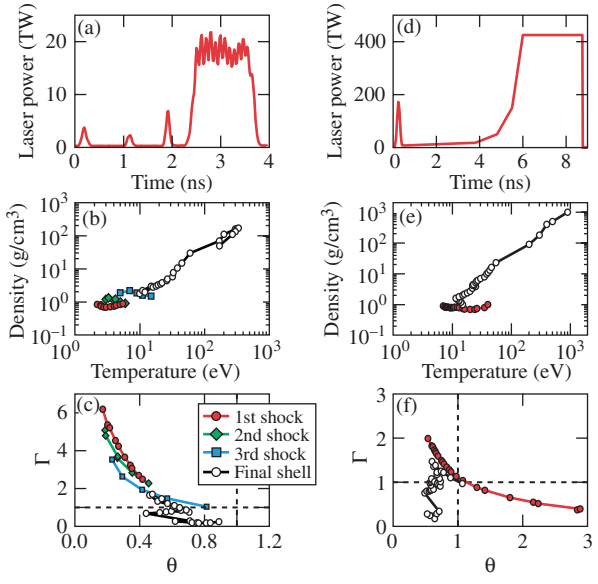

FIG. 1 (color online). (a)–(c) A cryogenic DT implosion on OMEGA; (d)–(f) a direct-drive ignition design for the NIF. In both cases, strongly coupled and degenerate plasma conditions are *indeed* accessed.

from 100 to 200 GPa has been measured using laser-driven shock waves [11–16], magnetically driven flyers [17,18], and convergent explosives [19,20]. Over the years, enormous theoretical efforts have been put forth to better understand the properties of deuterium under high pressure. The widely used *SESAME* EOS table of deuterium is based on the "chemical model" of matter [21,22], which has adopted liquid perturbation theory in the molecular or atomic fluid phase for ICF plasma conditions. The first-order expansion was originally used in the *SESAME* model [21] to take only the nearest-neighbor interactions into account, and did not fully account for the effects of strong coupling and many-body degeneracy in nonideal plasmas. *Ab initio* calculations for the deuterium EOS have been performed by using the method of density functional theory molecular dynamics (DFT-MD) [23–30] and the path integral Monte Carlo (PIMC) method [31–35]. These first-principles methods fully take coupling and degeneracy effects into account, in contrast to chemical models [21,22,36–38].

For ICF applications, we are especially concerned with the EOS accuracy along the implosion path in the density-temperature range of $\rho \sim 1.0$–1000 g/cm^3 and $T \sim 1.0$–1000 eV. For these plasma conditions (e.g., $T > 10$ eV), the DFT-based methods become impractical because of the huge number of electronic orbitals required [39], while the EOS can be derived efficiently with the PIMC method. In this Letter, we present a first-principles equation-of-state (FPEOS) table of deuterium from restricted PIMC calculations [40]. The same method has been successfully applied to compute the deuterium EOS up to a density of $\rho = 5.388$ g/cm^3 [33,41], which has been favorably compared with DFT-MD calculations [34]. We have used free-particle nodes to restrict the path propagation in order to construct an antisymmetric density matrix. The Coulomb interactions enter via a high-T pair-density matrix, $\rho(R, R'; \delta\beta)$. Using its convolution property, the density matrix $\rho(R, R'; \beta)$ can be expressed by

$$\rho(R, R'; \beta) = \int dR_1 dR_2 \ldots dR_{M-1} \rho(R, R_1; \delta\beta) \times \rho(R_1 R_2; \delta\beta) \ldots \rho(R_{M-1}, R'; \delta\beta) \quad (1)$$

with $\beta = 1/kT$ and $\delta\beta = \beta/M$, where M is the number of steps along the path in imaginary time. Monte Carlo methods are used to efficiently evaluate the multidimensional integral. Thermodynamic properties (associated with operator $\hat{O}$) are derived from

$$\langle \hat{O} \rangle = \frac{\int dR dR' \langle R|\hat{O}|R'\rangle\langle R'|\rho(R, R'; \beta)|R\rangle}{\int dR \langle R|\rho(R, R'; \beta)|R\rangle}. \quad (2)$$

We have performed our PIMC calculations with various numbers of atoms in periodic cubic simulation cells depending on density: 64 deuterium atoms for $\rho < 2.5$ g/cm^3, 128 atoms for $2.5 < \rho < 10.5$ g/cm^3, and 256 atoms for $\rho > 10.5$ g/cm^3. The time step $\delta\beta$ was chosen to be small enough, $1/\delta\beta > 75 \times kT_F$, so that interactions and degeneracy effects were accurately accounted for.

In Fig. 2(a), we compare the principal Hugoniot between our FPEOS table and the *SESAME* EOS for different temperatures marked on the curve. We have also plotted the previous Hugoniot calculated using the same PIMC method with 32 atoms and a time step of $1/\delta\beta = 8 \times 10^6$ K [33,41]. Good agreement is found with these previous PIMC calculations. Current PIMC simulations used 64 atoms and a smaller time step of $1/\delta\beta = 1.6 \times 10^7$ K. We found that deuterium is slightly softer, according to our PIMC calculations, than the *SESAME* prediction for pressures below ~2 Mbar, while it is stiffer in the pressure range of $\sim 2 < P < 100$ Mbar (the dynamic compression range in ICF). The PIMC predicted compression of $\rho/\rho_0 \approx 4.3$ below ~2 Mbar agrees with DFT-MD calculations [26,28] and EOS measurements using magnetically driven flyers [17,18]. It may also agree with the laser-shock results [15,16], as a correction to the quartz standard used in experiments suggests [42]. To give an interpretation of these discrepancies, in Figs. 2(b) and 2(c) we have plotted the relative differences in pressure and energy versus density for two temperatures, $T = 344.47$ eV and $T = 21.54$ eV. The statistical error bars of our PIMC results are also marked. At $T = 344.47$ eV, both the pressure and energy from PIMC and *SESAME* simulations are within ~1%. This is expected because plasmas at such high temperatures are classical ($\Gamma \ll 1$, $\theta \gg 1$). The PIMC and *SESAME* Hugoniot curves are identical above 344 eV, as shown in Fig. 2(a). For a lower temperature of 21.54 eV, however, the energy difference is larger, as indicated in Fig. 2(c). For the principal Hugoniot, in the density range of $\rho = 0.6$–0.8 g/cm^3, the internal energy in FPEOS is ~6% lower than that of *SESAME* (for this

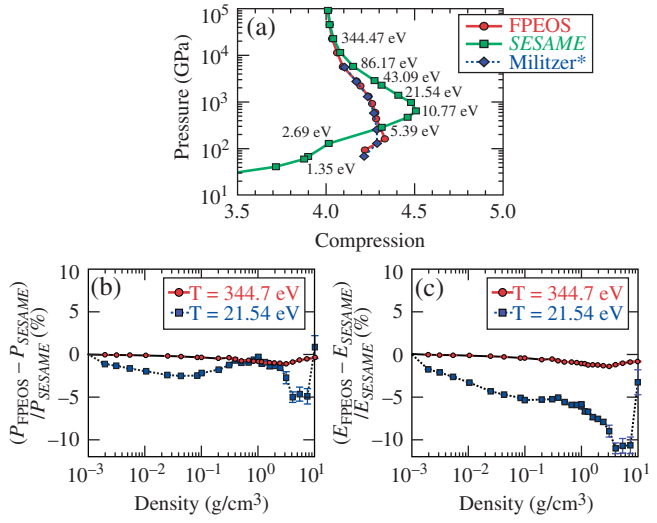

FIG. 2 (color online). (a) The principal Hugoniot for liquid deuterium. The relative deviation in (b) pressure and (c) energy between the FPEOS and *SESAME* as a function of density, for temperatures of 344.7 eV (red circles) and 21.54 eV (blue squares).

comparison, the zero energy has been set to the ground state of an isolated molecule, $E_0 = -15.886$ eV), even though the pressures agree within ~1%. According to the Hugoniot equation $[E_f - E_0 + (1/2)(P_f + P_0) \times (V_f - V_0) = 0]$, the final state can be expressed as $E_f + (1/2)P_f V_f \approx E_0 + (1/2)P_f V_0$ because of $P_f \gg P_0$, where (P_0, E_0, V_0) and (P_f, E_f, V_f) are the initial and final pressure, energy, and volume of deuterium. Therefore, with a similar value of P_f, the smaller E_f predicted by the FPEOS requires a larger V_f to satisfy the Hugoniot equation [43], thereby resulting in less compression, as seen in Fig. 2(a). Such a discrepancy was noticed by Kerley in 2003 [22], and with some improvements to the ionization equilibrium model, he succeeded in decreasing the *SESAME* compression to better agree with the first-principle calculations in this high-pressure (~ 10 Mbar) regime [22]. Figure 2(c) indicates that as the density increases, the relative deviation in energy reaches a maximum of ~11% around $\rho \sim 4$–5 g/cm^3 ($\Gamma \approx 1.3$ and $\theta \approx 0.4$) for $T = 21.54$ eV. The *SESAME* model again approaches PIMC calculations at very high densities (e.g., $\rho = 10$ g/cm^3), as local screening was correctly accounted for in chemical models [21,22].

From PIMC calculations, we have derived a first-principles EOS table for deuterium, which covers the typical ICF fuel conditions of $\rho = 0.002$–1596 g/cm^3 and $T = 1.35$ eV–5.5 keV. For each density, we have performed PIMC calculations towards the lowest temperature corresponding to $\theta = T/T_F \approx 0.1$. The high-temperature limit of $T > 5.5$ keV is obtained by linearly extrapolating (in T) the highest PIMC point, since ideal plasma conditions are expected at high temperatures.

With the FPEOS table and hydrocodes, we can now explore the implications of strong-coupling and degeneracy effects in ICF implosions. Results are shown in Figs. 3 and 4, respectively, for a cryogenic D_2 implosion ($\alpha \approx 2.5$) on the OMEGA Laser System and a direct-drive DT design on the NIF. We have used the 1D radiative hydrocode LILAC [44] to perform these simulations. In Fig. 3(a), we plot the pulse shape used for imploding a cryogenic D_2 target (877 μm diameter) with a 10 μm deuterated plastic ablator and 95 μm of D_2 ice. Figure 3(b) shows the density and temperature profiles at the end of the laser pulse ($t =$ 3.6 ns) from both the FPEOS and the *SESAME* based simulations. The shell's peak density and average temperature were $\rho_p \sim 5$ g/cm^3 and $T \sim 15$ eV, which correspond to the coupled and degenerate regimes with $\Gamma \approx 1.7$ and $\theta \approx 0.3$. It is shown that the FPEOS simulation predicted ~10% lower ρ_p but higher temperature relative to the *SESAME* prediction. As the Hugoniot comparison indicated in Fig. 2(a), the FPEOS is slightly stiffer than *SESAME* in this temperature range, which explains the lower ρ_p. The slightly higher temperature in the FPEOS case originated from the lower internal energy [see Fig. 2(c)]. Since the laser ablation does the same work/energy to the shell compression and its kinetic motion, a lower internal energy in FPEOS means more energy is partitioned to heat the shell, thereby resulting in a higher temperature. Such a temperature increase and density drop can have consequences in the implosion performance. At the stagnation stage (peak compression), Fig. 3(c) shows that the peak density is ~30% lower according to FPEOS ($\rho_p \approx 90$ g/cm^3) compared to *SESAME* ($\rho_p \approx 130$ g/cm^3). The peak areal density $(\rho R)_p$ and neutron yield were also reduced by ~10%–20%, as shown in Fig. 3(d). The neutron-averaged areal density $\langle \rho R \rangle$ predicted with FPEOS was ~198 mg/cm^2, which is in better agreement with the experimentally measured value of $\langle \rho R \rangle_n = 202 \pm 7$ mg/cm^2 [45], in contrast to the *SESAME* prediction of $\langle \rho R \rangle = 247$ mg/cm^2. Nonuniformities of laser and target cannot account for the large

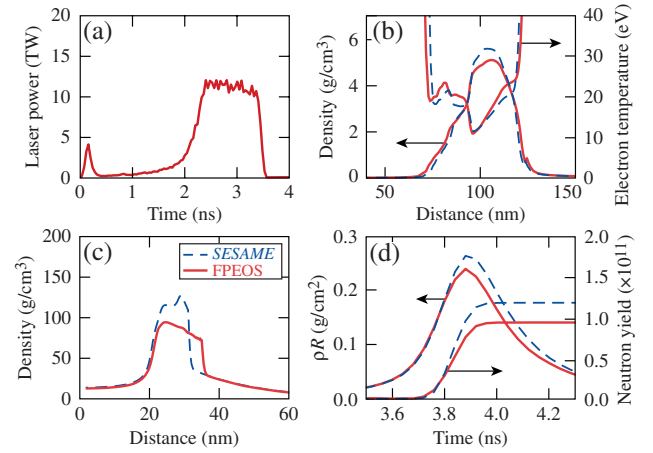

FIG. 3 (color online). The hydrocode simulations of a cryogenic D_2 implosion on OMEGA using the FPEOS table (red solid line) and the *SESAME* EOS table (blue dashed line): (a) the laser pulse shape; (b) the density-temperature profiles of the imploding D_2 shell at the end of the laser pulse ($t = 3.6$ ns); (c) the density profile at the peak compression; and (d) the areal density (ρR) and neutron yield as a function of time.

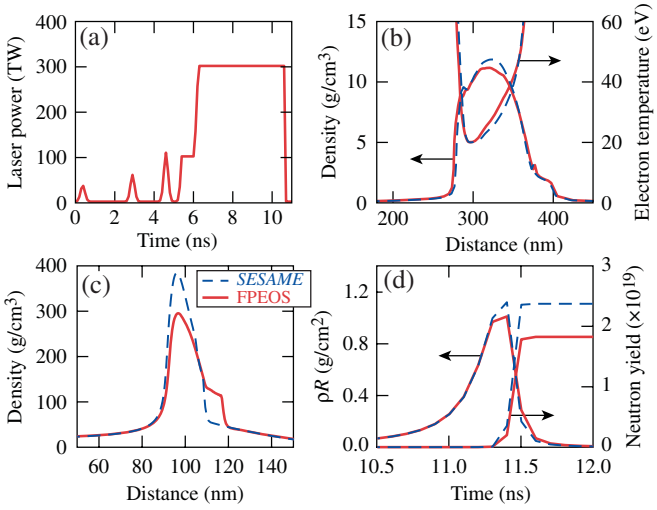

FIG. 4 (color online). Similar to Fig. 3 but for a NIF direct-drive ignition design.

discrepancy between measurements and *SESAME* predictions, as we have noted that these perturbations in experiments can reduce the neutron yield [46] but hardly affect the compression ρR.

A similar effect of strong coupling and degeneracy was also seen for the NIF designs. Figure 4 shows an example for a NIF target ($\phi = 3.37$ mm) having a 37 μm plastic ablator and 150 μm of DT ice. At the end of the laser pulse [$t = 10.7$ ns in Fig. 4(b)], we also found a decrease in ρ_p and a temperature increase for the FPEOS relative to *SESAME* simulations. The peak density near the stagnation dropped from 383 (*SESAME*) to 294 g/cm^3 (FPEOS), as is indicated by Fig. 4(c). The resulting ρR and neutron yield as a function of time is plotted in Fig. 4(d). The peak ρR changed from 1.1 (*SESAME*) to 1.0 g/cm^2 (FPEOS), while the yield dropped from the *SESAME* value of $Y = 2.4 \times 10^{19}$ to 1.8×10^{19} for the FPEOS simulation. Consequently, the energy gain dramatically decreased from 45 (*SESAME*) to 34 (FPEOS). This implies that such an accurate FPEOS table is essentially important for low-adiabat ($\alpha \leq 2$) ICF designs, as plasmas in low-adiabat imploding shells access more strongly coupled and degenerate regimes.

In summary, we have derived a first-principles equation-of-state table of deuterium for ICF applications from PIMC calculations. The FPEOS table covers the typical fuel density and temperature conditions in ICF implosions. In comparison with the *SESAME* table, the FPEOS predicts $\sim$10% lower internal energy but comparable pressure (within a few percent) for strongly coupled and degenerate plasma conditions. Hydrosimulations using the FPEOS table indicate significant decreases in the predicted peak density ($\sim$ 30%–40%). The results also show a reduction in the peak areal density ρR($\sim$10%) and the neutron yield (energy gain) by $\sim$20% with respect to the corresponding *SESAME* simulations. The compression (ρR) predicted from FPEOS agrees better with experiments. It is noted that the extreme conditions covered in the FPEOS table are also important in astrophysics, for example, to model the evolution of stars [47] and to understand the thermodynamical properties of stellar matter [48].

This work was supported by the U.S. Department of Energy Office of Inertial Confinement Fusion under Cooperative Agreement No. DE-FC52-08NA28302, the University of Rochester, and New York State Energy Research and Development Authority. S. X. H. would like to thank the National Science Foundation (NSF) for support under the NSF-TeraGrid Grants No. PHY090093 and No. PHY100003. This work was partially conducted utilizing the NICS's Kraken Supercomputer. B. M. acknowledges support from the University of California Laboratory Free Research Program, the NSF, and NASA.

*E-mail: shu@lle.rochester.edu

[1] S. Atzeni and J. Meyer-ter-Vehn, *The Physics of Inertial Fusion* (Clarendon Press, Oxford, 2004).
[2] R. L. McCrory *et al.*, Phys. Plasmas **15**, 055503 (2008).
[3] J. D. Lindl, Phys. Plasmas **2**, 3933 (1995).
[4] S. X. Hu *et al.*, Phys. Rev. Lett. **100**, 185003 (2008).
[5] S. X. Hu *et al.*, Phys. Rev. Lett. **101**, 055002 (2008).
[6] T. R. Boehly *et al.*, Opt. Commun. **133**, 495 (1997).
[7] J. Paisner, Laser Focus World **30**, 75 (1994).
[8] M. S. Murillo and M. W. C. Dharma-wardana, Phys. Rev. Lett. **100**, 205005 (2008); B. Jeon *et al.*, Phys. Rev. E **78**, 036403 (2008); L. X. Benedict *et al.*, Phys. Rev. Lett. **102**, 205004 (2009).
[9] V. Recoules *et al.*, Phys. Rev. Lett. **102**, 075002 (2009).
[10] E. L. Pollock and B. Militzer, Phys. Rev. Lett. **92**, 021101 (2004).
[11] L. B. Da Silva, Phys. Rev. Lett. **78**, 483 (1997).
[12] G. W. Collins *et al.*, Science **281**, 1178 (1998).
[13] G. W. Collins, Phys. Plasmas **5**, 1864 (1998).
[14] A. N. Mostovych *et al.*, Phys. Rev. Lett. **85**, 3870 (2000).
[15] T. R. Boehly *et al.*, Phys. Plasmas **11**, L49 (2004).
[16] D. G. Hicks *et al.*, Phys. Rev. B **79**, 014112 (2009).
[17] M. D. Knudson *et al.*, Phys. Rev. Lett. **87**, 225501 (2001).
[18] M. D. Knudson *et al.*, Phys. Rev. B **69**, 144209 (2004).
[19] S. I. Belov *et al.*, JETP Lett. **76**, 433 (2002).
[20] V. E. Fortov *et al.*, Phys. Rev. Lett. **99**, 185001 (2007).
[21] G. I. Kerley, Phys. Earth Planet. Inter. **6**, 78 (1972).
[22] G. I. Kerley, SNL Report No. SAND2003-3613, 2003 (unpublished).
[23] L. Collins *et al.*, Phys. Rev. E **52**, 6202 (1995).
[24] T. J. Lenosky *et al.*, Phys. Rev. B **61**, 1 (2000).
[25] G. Galli *et al.*, Phys. Rev. B **61**, 909 (2000).
[26] L. A. Collins *et al.*, Phys. Rev. B **63**, 184110 (2001).
[27] J. Clérouin and J.-F. Dufrêche, Phys. Rev. E **64**, 066406 (2001).
[28] M. P. Desjarlais, Phys. Rev. B **68**, 064204 (2003).
[29] S. A. Bonev, B. Militzer, and G. Galli, Phys. Rev. B **69**, 014101 (2004).
[30] S. A. Bonev *et al.*, Nature (London) **431**, 669 (2004).
[31] C. Pierleoni *et al.*, Phys. Rev. Lett. **73**, 2145 (1994).
[32] W. R. Magro *et al.*, Phys. Rev. Lett. **76**, 1240 (1996).
[33] B. Militzer and D. M. Ceperley, Phys. Rev. Lett. **85**, 1890 (2000).
[34] B. Militzer *et al.*, Phys. Rev. Lett. **87**, 275502 (2001).
[35] V. Bezkrovniy *et al.*, Phys. Rev. E **70**, 057401 (2004).
[36] D. Saumon and G. Chabrier, Phys. Rev. A **46**, 2084 (1992).
[37] M. Ross, Phys. Rev. B **58**, 669 (1998).
[38] F. J. Rogers, Contrib. Plasma Phys. **41**, 179 (2001).
[39] L. A. Collins (private communication).
[40] D. M. Ceperley, Rev. Mod. Phys. **67**, 279 (1995).
[41] B. Militzer, Ph.D. thesis, University of Illinois at Urbana-Champaign, 2000.
[42] M. D. Knudson and M. P. Desjarlais, Phys. Rev. Lett. **103**, 225501 (2009).
[43] B. Militzer, Phys. Rev. Lett. **97**, 175501 (2006).
[44] J. Delettrez, Phys. Rev. A **36**, 3926 (1987).
[45] T. C. Sangster *et al.*, Phys. Rev. Lett. **100**, 185006 (2008).
[46] S. X. Hu *et al.*, Phys. Plasmas **16**, 112706 (2009).
[47] F. J. Rogers and A. Nayfonov, Astrophys. J. **576**, 1064 (2002).
[48] W. Stolzmann and T. Blöcker, Astron. Astrophys. **361**, 1152 (2000).